



Multiphoton double ionization of helium by ultrashort XUV pulses: Probing the role of electron correlations

Wei-Chao Jiang ^{1,2,*}, Manuel Ederer,^{3,2} Stefan Donsa,² Johannes Feist ⁴, Iva Březinová,²
Christoph Lemell,² and Joachim Burgdörfer²

¹*Institute of Quantum Precision Measurement, College of Physics and Optoelectronic Engineering,
Shenzhen University, Shenzhen 518060, China*

²*Institute for Theoretical Physics, Vienna University of Technology,
Wiedner Hauptstraße 8-10, A-1040 Vienna, Austria, EU*

³*University Service Centre for Transmission Electron Microscopy, Vienna University of Technology,
Wiedner Hauptstraße 8-10, A-1040 Vienna, Austria, EU*

⁴*Departamento de Física Teórica de la Materia Condensada and Condensed Matter Physics Center (IFIMAC),
Universidad Autónoma de Madrid, 28049 Madrid, Spain, EU*



(Received 24 February 2023; revised 28 June 2023; accepted 17 July 2023; published 2 August 2023)

We investigate multiphoton double ionization of helium by ultrashort XUV pulses involving up to 5 XUV photons by numerically solving the time-dependent Schrödinger equation for helium in its full dimensionality. We explore the crucial role of dynamical electron correlations by systematically varying the pulse duration and the number of absorbed photons. With increasing photon number, a multitude of ionization pathways opens up. The relative importance of correlations varies with pulse duration. Even in the spectrally sequential regime, correlation effects become increasingly important as the pulse duration becomes shorter and as the number of absorbed photons is increased. We identify a pathway to double ionization (DI) involving correlated excitation ionization as an intermediate step which can provide a contribution to the total DI yield comparable to the conventional direct sequential double ionization. Supported by concurrent classical trajectory Monte Carlo simulations, we identify strong electron-electron correlations in double ionization even at large distances from the nucleus.

DOI: [10.1103/PhysRevA.108.023102](https://doi.org/10.1103/PhysRevA.108.023102)

I. INTRODUCTION

Electron-electron correlations play an important role in many physical processes of multielectron systems. Their satisfactory description is often quite challenging. Double ionization (DI) of the helium atom by light fields or charged particles represents one of the simplest prototypical cases for which dynamical correlations have been extensively studied, both experimentally and theoretically [1–5]. For the description of the most fundamental perturbative limit of one-photon double ionization (1PDI), inclusion of correlation is even *conditio sine qua non*, as on the Hartree-Fock level only shake-off processes would occur [3,4,6–9]. 1PDI has attracted considerable attention over the last few decades [3,4,10–13]. The recent renewed interest in 1PDI is stimulated in part by the availability of high-intensity, high-energy photon beams at free-electron laser (FEL) sources [14–17], which enables the in-depth exploration of nondipole effects.

In the opposite strong-field limit, i.e., the nonperturbative strong-field double ionization (SFDI) by intense infrared (IR) laser pulses, correlation effects have been identified in terms of the prominent “knee” structure [18–20] in the total DI yield as a function of intensity, signifying nonsequential

double ionization (NSDI) by electron impact ionization of the second electron following ionization and acceleration of the first electron. Correlated as well as anticorrelated electron emission could be identified in joint momentum spectra along the laser polarization axis [21–27], and simplified classical and quantum models have been employed to shed light on the underlying final-state correlation effects [28–34]. Fully *ab initio* quantum simulations in their full dimensionality of the strong-field regime still represent a major challenge and only a few pioneering results have recently become available [35,36].

Multiphoton double ionization (MPDI) bridges the gap between the perturbative 1PDI and highly nonperturbative SFDI limits. The recent availability of strong XUV pulses generated by FEL [17,37–39] and high-order-harmonic generation (HHG) [40–42] have opened up opportunities to study MPDI processes previously only sparingly explored experimentally. For MPDI, the full numerical solution of the time-dependent Schrödinger equation (TDSE) is still within reach and accurate theoretical predictions are still feasible. Most studies have so far focused on the simplest MPDI, i.e., two-photon double ionization (2PDI) of helium [11,12,43–80] or of heliumlike ions [81]. Traditionally, the borderline between strongly and weakly correlated 2PDI is considered to lie in the spectral domain at the XUV photon energy of the second ionization potential of He [i.e., the ionization potential of He⁺

*jiang.wei.chao@szu.edu.cn

(1s)], $\hbar\omega_{\text{XUV}} = I_2 = 54.4$ eV. Above I_2 , double ionization can occur by sequential ionization of He and He⁺ following the successive absorption of two temporally separated photons. Conversely, for photon energies in between half of the threshold for double ionization, $I_{\text{DI}} = I_1 + I_2$ and I_2 , $I_{\text{DI}}/2 < \hbar\omega_{\text{XUV}} < I_2$, only NSDI can take place as the two electrons in the exit channel must share the energy delivered by the two photons in order to jointly escape. Dynamical final-state correlations are therefore a prerequisite for NSDI to unfold. For ultrashort XUV pulses with pulse durations T_p in the attosecond regime, however, this spectral borderline between uncorrelated sequential double ionization (SDI) and NSDI becomes blurred and even hardly observable [67]. This is not only due to the large spectral Fourier width of the ultrashort pulse ($\Delta\omega \sim 1/T_p$) simultaneously covering both the sequential and nonsequential spectral regimes. Conceptually and more importantly, strong electron-electron correlation develops in the time domain as the two electrons must escape from the atom in close temporal (limited by T_p) and spatial proximity. Consequently, even for photon energies well above I_2 , the nominally sequential ejection of the two electrons will be confined to a small time interval, rendering the electron-electron correlation effects prominent [67]. The single-ionization continuum has been recognized as the dominant intermediate state in either sequential or nonsequential 2PDI. Therefore, a virtual sequential picture [37,51,73,74] is able to provide a unified description for both sequential and nonsequential 2PDI.

Multiphoton double ionization involving more than $n_{\text{ph}} = 2$ XUV photons has so far been the focus of only a few theoretical [82–87] and experimental [88,89] works where photoabsorption of up to $n_{\text{ph}} = 5$ photons was considered. Both solutions of the full-dimensional TDSE [36,82–84] as well as of a one-dimensional model [85] provide information on the total DI probability as well as on the angular distributions. Exploiting the resonant two-photon excitation, strong deviations from the intensity scaling $\propto I^5$ expected for a perturbative 5PDI process were found in the experiment [89] when the XUV photon energy was tuned across the resonant two-photon excitation in He⁺ [$1s \rightarrow 2s$]. In the present work, our aim is to systematically explore the MPDI of helium involving up to five photons as a function of the duration T_p of the ultrashort attosecond to femtosecond XUV pulse which, so far, has not received extensive attention. We focus on the role of electron correlations in both the time and spectral domains for these higher-order photon processes where a multitude of pathways can contribute. Even though these pathways represent spectrally sequential processes, dynamical correlation effects can become increasingly important. We identify a previously neglected pathway to DI involving a correlated excitation-ionization process as an intermediate step that can be as important as the conventional direct sequential double-ionization process.

The structure of the present paper is as follows: In Sec. II, we briefly review the methods for the numerical solution of the TDSE and extraction of the double-ionization signal and discuss extensions required for MPDI. An overview over possible pathways to double ionization by a multiphoton process is given in Sec. III. Numerical results for the angle-integrated and angle-resolved photoelectron spectra as well as

momentum correlation functions will be presented in Sec. IV. Concluding remarks are given in Sec. V. Atomic units are used unless stated otherwise.

II. THEORETICAL METHODS

Our description of MPDI is based on the numerical solution of the TDSE of helium in its full dimensionality,

$$i\frac{\partial}{\partial t}\Psi(\mathbf{r}_1, \mathbf{r}_2, t) = [H_0 + H_1(t)]\Psi(\mathbf{r}_1, \mathbf{r}_2, t), \quad (1)$$

where H_0 represents the field-free Hamiltonian of helium which fully includes the electron-electron repulsive potential, and $H_1(t)$ represents the electron-laser interaction Hamiltonian given in the velocity gauge by

$$H_1(t) = -i\mathbf{A}(t) \cdot (\nabla_1 + \nabla_2). \quad (2)$$

The vector potential \mathbf{A} is assumed to have a cosine-squared pulse envelope and is linearly polarized along the z axis,

$$\mathbf{A}(t) = A_0 \cos^2\left(\frac{\pi t}{T_p}\right) \cos(\omega_{\text{XUV}}t)\hat{z}, \quad (3)$$

where T_p is the total pulse duration and the full width at half maximum (FWHM) of the pulse envelope is $T_p/2$. The vector potential \mathbf{A} is nonzero for $-\frac{T_p}{2} < t < \frac{T_p}{2}$, and ω_{XUV} is the photon energy. The electric field \mathbf{F} is related to the vector potential through $\mathbf{F} = -d\mathbf{A}/dt$. The pulse intensity I is fixed in this paper at $I = 10^{14}$ W/cm². We note, however, that most of the results presented below do *not* strongly depend on the precise value of I .

In the present TDSE approach [12,55,56,90], the wave function $\Psi(\mathbf{r}_1, \mathbf{r}_2, t)$ is expressed in terms of a time-dependent close-coupling (TDCC) expansion,

$$\Psi(\mathbf{r}_1, \mathbf{r}_2, t) = \sum_{L,M,l_1,l_2} \frac{R_{l_1,l_2}^{L,M}(r_1, r_2, t)}{r_1 r_2} Y_{l_1,l_2}^{L,M}(\hat{r}_1, \hat{r}_2), \quad (4)$$

where $Y_{l_1,l_2}^{L,M}(\hat{r}_1, \hat{r}_2)$ are the coupled spherical harmonics. For the linearly polarized laser light, only the partial waves with magnetic quantum number $M = 0$ are involved in double ionization from the ground state of helium. In most of the calculations presented in the following, we include in Eq. (4) partial waves up to $l_{1,2} \leq 8$ and total angular momenta up to $L = n_{\text{ph}} + 1$ for most n_{ph} PDI, to avoid spurious contributions due to truncation effects and find convergence for the angular distributions. However, in cases where double ionization gives rise to electron-electron scattering at large distances from the nucleus, as demonstrated below, considerably larger $l_{1,2}$ need to be included. We include $l_{1,2}$ up to 40 in the present calculations of 3PDI. The radial wave functions $R_{l_1,l_2}^{L,M}(r_1, r_2, t)$ are discretized in terms of the finite-element discrete-variable representation (FEDVR) method [91–93]. The split-Lanczos algorithm [94–98] is used for the time propagation.

For long pulses in the multifemtosecond regime, used here to explore the spectrally sequential regime, it is necessary to follow the two-electron wave packet over large distances from the ionic core. Therefore, a large computational box is required to represent the wave packet. One popular method that is widely applied in solutions of the

one-electron TDSE to overcome this numerical difficulty is the wave-splitting method [99], in which the outer part of the photoelectron wave packet is collected over a short time interval of propagation. Here we extend this wave-splitting method to the DI of helium. In comparison with the recently developed time-dependent surface flux (tSurff) method [36], a perfect absorber such as infinite-range exterior complex scaling (irECS) [100] is not necessary for our method. We note that the application of irECS will result in a non-Hermitian Hamiltonian, which renders the application of the efficient Lanczos time propagator [94–98] difficult. Accordingly, the wave function $\Psi(\mathbf{r}_1, \mathbf{r}_2)$ is split into the inner part $\Psi_{\text{in}}(\mathbf{r}_1, \mathbf{r}_2)$ periodically in time with a period of 10 a.u. through application of the split operation S at time t ,

$$\Psi_{\text{in}}(\mathbf{r}_1, \mathbf{r}_2, t) = S(r_1)S(r_2)\Psi(\mathbf{r}_1, \mathbf{r}_2, t). \quad (5)$$

The smoothness of the split is controlled by the width Δ in

$$S(r) = \frac{1}{1 + e^{(r-R_c)/\Delta}}. \quad (6)$$

R_c determines the borderline between the inner and outer regions. Its typical value used in most of the present calculations is $R_c = 220$ a.u. For the 5PDI at the longest pulse duration, we take R_c to be 500 a.u. In cases with strong electron-electron interaction at large distances in the exit channel, we use R_c up to 600 a.u. Absorbing masking functions are applied at larger radii.

Only the inner part of the wave function, $\Psi_{\text{in}}(\mathbf{r}_1, \mathbf{r}_2, t)$, is kept in the propagation by the full Hamiltonian $H_0 + H_1(t)$, while the propagation of the outer part of the wave function,

$$\Psi_{\text{out}}(\mathbf{r}_1, \mathbf{r}_2, t) = \Psi(\mathbf{r}_1, \mathbf{r}_2, t) - \Psi_{\text{in}}(\mathbf{r}_1, \mathbf{r}_2, t), \quad (7)$$

is approximated by a Volkov propagator. Specifically, the DI amplitude at time t_i is obtained by projecting the outer wave function onto the double-ionization continuum,

$$f(\mathbf{k}_1, \mathbf{k}_2, t_i) = \langle \Phi_{\mathbf{k}_1, \mathbf{k}_2} | \Psi_{\text{out}}(\mathbf{r}_1, \mathbf{r}_2, t_i) \rangle, \quad (8)$$

with the double-ionization continuum $|\Phi_{\mathbf{k}_1, \mathbf{k}_2}\rangle$ constructed as the symmetric product of two hydrogenlike scattering states for nuclear charge 2. The total DI amplitude at the final time t_f is expressed as

$$f(\mathbf{k}_1, \mathbf{k}_2) = \sum_i U_{\mathbf{k}_1, \mathbf{k}_2}(t_i, t_f) f(\mathbf{k}_1, \mathbf{k}_2, t_i), \quad (9)$$

with

$$U_{\mathbf{k}_1, \mathbf{k}_2}(t_i, t_f) = e^{-i \int_{t_i}^{t_f} [\frac{k_1^2 + k_2^2}{2} + \mathbf{A}(\tau) \cdot (\mathbf{k}_1 + \mathbf{k}_2)] d\tau} \quad (10)$$

the time evolution factor expressed in terms of the Volkov phases of the two photoelectrons accumulated between times t_i and t_f .

Alternatively, Eq. (9) can be calculated iteratively,

$$\mathcal{F}_{i+1}(\mathbf{k}_1, \mathbf{k}_2) = U_{\mathbf{k}_1, \mathbf{k}_2}(t_i, t_{i+1}) \mathcal{F}_i(\mathbf{k}_1, \mathbf{k}_2) + f(\mathbf{k}_1, \mathbf{k}_2, t_{i+1}), \quad (11)$$

starting from

$$\mathcal{F}_1(\mathbf{k}_1, \mathbf{k}_2) = f(\mathbf{k}_1, \mathbf{k}_2, t_1), \quad (12)$$

and resulting in

$$f(\mathbf{k}_1, \mathbf{k}_2) = \mathcal{F}_f(\mathbf{k}_1, \mathbf{k}_2). \quad (13)$$

Finally, the fully differential vectorial joint momentum distribution of the two ejected electrons follows from

$$P(\mathbf{k}_1, \mathbf{k}_2) = |f(\mathbf{k}_1, \mathbf{k}_2)|^2. \quad (14)$$

We note that the single-ionization component of the two-electron wave function included in the outer wave function $\Psi_{\text{out}}(\mathbf{r}_1, \mathbf{r}_2, t_i)$ could be further promoted to the double-ionization continuum at a larger time $t > t_i$. Such contributions to DI are neglected in the present calculations. However, their weight is expected to be small for sufficiently large R_c . The present protocol [Eqs. (9) and (13)] is particularly useful for the field-free propagation, during which the single-ionization continuum in $\Psi_{\text{out}}(\mathbf{r}_1, \mathbf{r}_2, t_i)$ obviously does not couple to the double-ionization continuum. The field-free propagation after the end of the pulse is necessary to reduce the error caused by approximating the double-ionization scattering state by the symmetric product of two hydrogenlike scattering states. For most calculations, we take the time of field-free propagation to be 50 a.u. with the split time interval unchanged. When strong dynamical correlations persist over large distances, we follow the field-free propagation for times up to $t_{\text{max}} = 500$ a.u. When collecting the double-ionization amplitude from the final wave function at time t_f , we use a smaller inner box, $R_c = 20$ a.u., for the split to make sure that the ionizing portion of the wave function has reached the outer region while most of the bound-state portion is still in the inner region. The persistence of dynamical correlations over large distances limits the range of applicability of the present approach to numerically solve Eq. (1) using the TDCC expansion, given by Eq. (4). We therefore perform, in addition, classical trajectory Monte Carlo (CTMC) simulations [101–103], which aid in the interpretation of the quantum simulations and allow for an approximate analysis of Coulomb correlation effects at large distances when convergence of the full quantum simulation can no longer be reached.

III. PATHWAYS FOR MULTIPHOTON DOUBLE IONIZATION

While for 2PDI of helium a clear spectral dividing line between sequential (S) and nonsequential (NS) DI is given by $\omega_{\text{XUV}} = I_2$, for higher-order processes involving $n_{\text{ph}} \geq 3$ photons, sequential and nonsequential processes become intertwined as a multitude of pathways emerge. A sample of those pathways for MPDI ranging from 2PDI to 5PDI is sketched in Fig. 1. With increasing number of photons and, correspondingly, decreasing energy per photon, resonant one-photon or resonant multiphoton intermediate states become available. An example of this, for 5PDI, was experimentally studied by Hikosaka *et al.* [89], who employed photons with $\omega_{\text{XUV}} = 20.4$ eV which allows for a resonant two-photon excitation $\text{He}^+ [1s \rightarrow 2s]$. In order to maximize the degree of nonsequentiality and correlation effects for these high-order processes, our choice of photon energies attempts to minimize resonant effects subject to the limitations given by the Fourier width of the ultrashort pulses. We also note that the contributions involving doubly excited states (DES) as intermediate states are weak. We choose,

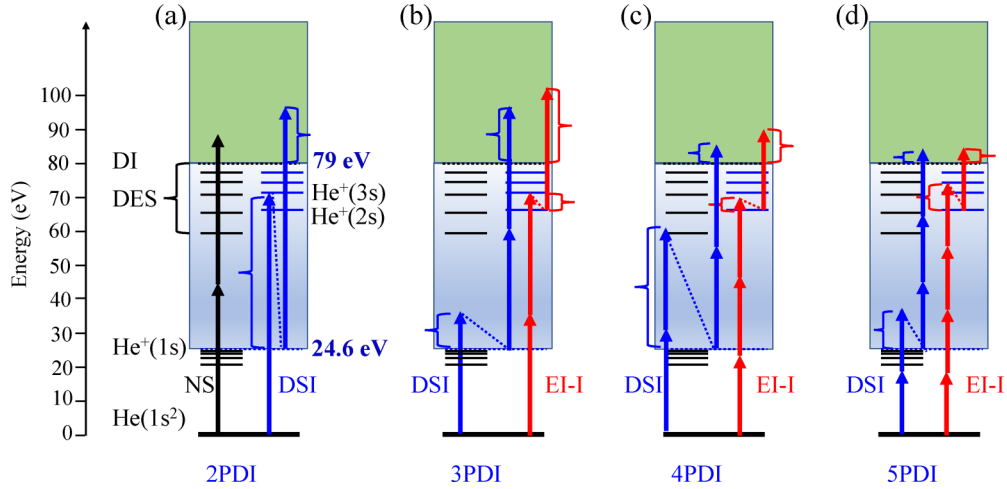


FIG. 1. Pathways for multiphoton double ionization (MPDI) of helium. (a) Sequential (blue) and nonsequential (black) 2PDI; (b) direct sequential ionization (DSI) (blue) and excitation-ionization (EI-I) (red) pathways for 3PDI; (c) DSI (blue) and EI-I (red) pathways for 4PDI; and (d) DSI (blue) and EI-I (red) pathways for 5PDI. For clarity, the EI-I process also allowed in 2PDI is omitted since it is much weaker than the DSI path in 2PDI. In each frame, the region of yellow-green color represents the double-ionization (DI) continuum, while levels close to DI on the left side are the doubly excited states (DES).

in the following, $\omega_{\text{XUV}} = 70$ eV in the spectrally sequential and 45 eV in the nonsequential regime for 2PDI, $\omega_{\text{XUV}} = 35$ eV for 3PDI, $\omega_{\text{XUV}} = 22$ eV for 4PDI, and $\omega_{\text{XUV}} = 18$ eV for 5PDI. We vary the pulse duration T_p by varying the number of optical cycles, thereby keeping the relative Fourier width $\Delta\omega/\omega$ of the pulse for different photon energies constant.

With increasing photon order, nonsequential processes begin to significantly contribute to pathways that nominally qualify as sequential. For example, for 3PDI, the standard direct sequential ionization (DSI) pathway entails the absorption of one 35 eV photon to reach the $\text{He}^+(1s)$ continuum, followed by a two-photon absorption event with $70 \text{ eV} > I_2$ reaching the two-electron continuum. However, an alternative pathway opens up, consisting of a correlated two-photon excitation ionization (EI) to $\text{He}^+(2s)$, followed by one-photon ionization (I) of the excited He^+ [Fig. 1(b)]. As the EI step is nonresonant, redistribution of the photon energy by electron-electron interaction is crucial for this two-electron process to unfold. As will be shown below, this EI-I process can be unambiguously identified and the competition between the DSI and the EI-I pathways will leave its mark on the two-electron spectra and joint angular distributions. Similar as well as more complex pathways appear for high-order processes [Figs. 1(c) and 1(d)]. Moreover, for ultrashort attosecond pulses, the (partial) sequentiality implied by the pathways, as indicated in the spectral domain (Fig. 1), is expected to be blurred and strong temporal correlations are expected to appear. The large Fourier width $\Delta\omega$ of the ultrashort pulse with T_p in the (sub)femtosecond domain leads to another remarkable feature in the two-electron spectra. As the effective spectral width for the n_{ph} -photon process scales approximately as $\Delta\omega_n \propto \sqrt{n_{\text{ph}}}\Delta\omega$, the two-electron spectra from both the n_{ph} PDI and $(n_{\text{ph}} - 1)$ PDI may coexist or even overlap. Indications of the simultaneous presence of DI by different photon orders will be given below.

IV. NUMERICAL RESULTS

A. Two-electron spectra

Since different ionization pathways of MPDI will, in general, result in different energy distributions of the emitted electrons, these paths can be most easily identified through the joint energy distribution $P(E_1, E_2)$, in the following represented by the joint radial momentum distribution $P(k_1, k_2)$ determined by integration over all emission angles of the two electrons,

$$P(k_1, k_2) = \int P(\mathbf{k}_1, \mathbf{k}_2) k_1 k_2 \sin \theta_1 \sin \theta_2 d\theta_1 d\theta_2 d\phi_1 d\phi_2. \quad (15)$$

In terms of $P(k_1, k_2)$, the total double-ionization probability P is given by

$$P = \int P(k_1, k_2) k_1 k_2 dk_1 dk_2. \quad (16)$$

The joint momentum distributions $P(k_1, k_2)$ for MPDI from two to five photons are shown in Fig. 2 at three different pulse durations, $T_p = 5, 20,$ and 100 cycles. The corresponding absolute durations and spectral widths are listed in Table I. The photon energies are chosen to avoid direct resonant coupling to the doubly excited states, but have no particular significance otherwise. Well-separated peaks in the $k_1 - k_2$ plane on a circle with $k_1^2 + k_2^2 = \text{const}$ appear most clearly for the longest pulses, $T_p = 100$ cycles with the smallest spectral width. The latter results in narrow sequential peaks (third row of Fig. 2). To render the peak positions easily visible, we plot the normalized single-electron momentum spectra $P(k_1)$, which are defined as

$$P(k_1) = \int P(k_1, k_2) k_2 dk_2, \quad (17)$$

in the fourth row of Fig. 2. In Fig. 2, we also give the total DI probability [Eq. (16)] to provide an indication for the absolute scale of these processes.

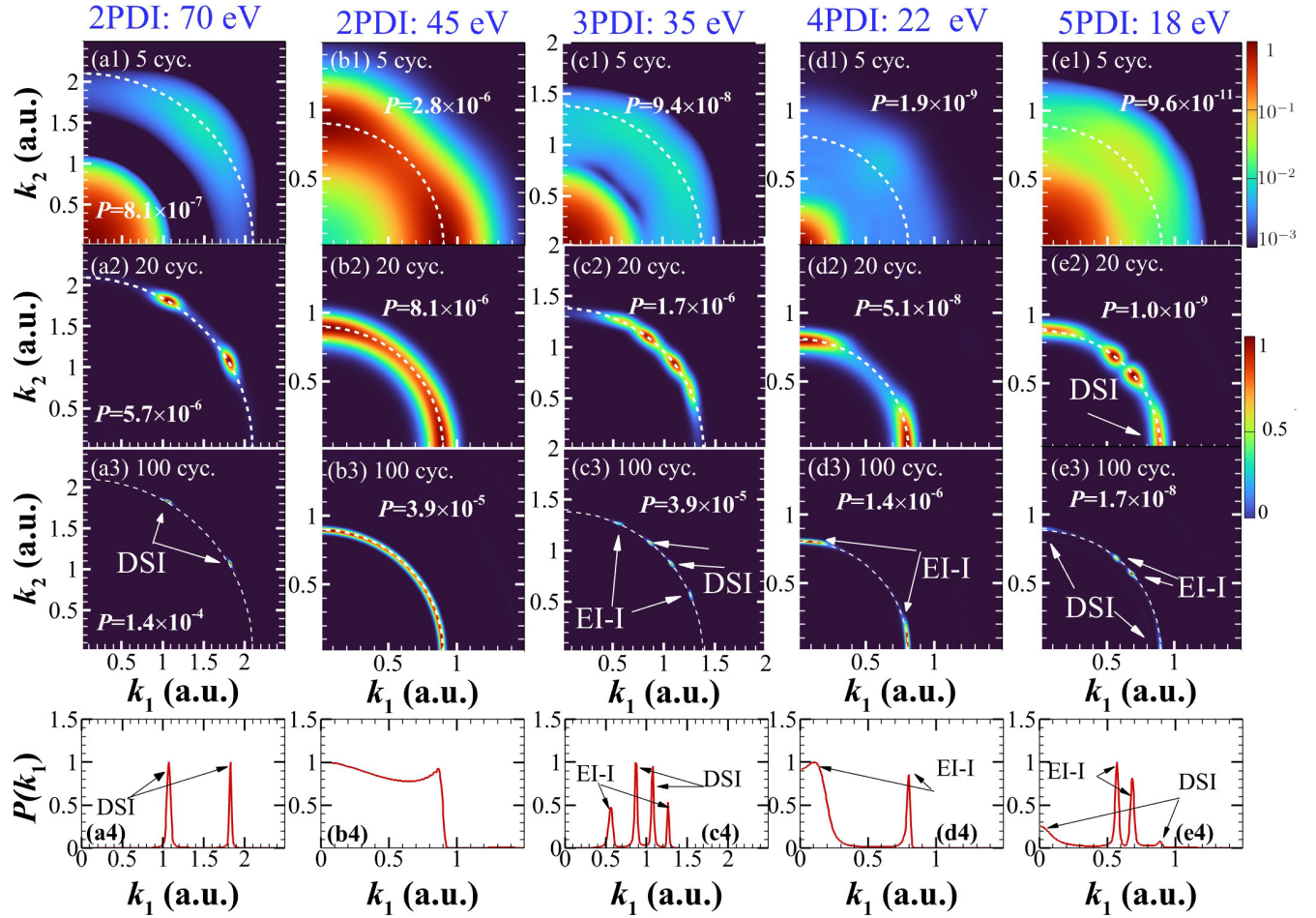


FIG. 2. Joint radial momentum distributions $P(k_1, k_2)$ [Eq. (15)] for (a1)–(a3) sequential 2PDI at photon energies of 70 eV, (b1)–(b3) nonsequential 2PDI at 45 eV, (c1)–(c3) 3PDI at 35 eV, (d1)–(d3) 4PDI at 22 eV, and (e1)–(e3) 5PDI at 18 eV. In each column, results for three pulse durations of $T_p = 5$ (first row), $T_p = 20$ (second row), and $T_p = 100$ (third row) cycles are shown. We use a logarithmic color scale in frames (a1), (c1), and (e1) to render the n_{ph} PDI process relative to the $(n_{\text{ph}} - 1)$ PDI visible and a relative decimal color scale in all other frames. In (a4), (b4), (c4), and (d4), the normalized single-electron radial momentum spectra $P(k_1)$ [Eq. (17)] at $T_p = 100$ cycles are given for each photon energy. To provide an absolute scale, we also give, in each frame, the value for the total probability P [Eq. (16)].

TABLE I. The photon energy ω_{XUV} , number of cycles, n_c , pulse duration T_p , and spectral width $\Delta\omega_{\text{XUV}} = 1.44\omega_{\text{XUV}}/n_c$ of the laser pulses in the present calculations.

ω_{XUV} (eV)	n_c	T_p (fs)	$\Delta\omega_{\text{XUV}}$ (eV)
70	5	0.3	20.2
70	20	1.2	5.0
70	100	5.9	1.0
45	5	0.46	13.0
45	20	1.8	3.2
45	100	9.2	0.65
35	5	0.59	10.1
35	20	2.4	2.52
35	100	11.8	0.5
22	5	0.94	6.3
22	20	3.8	1.6
22	100	18.8	0.32
18	5	1.15	5.2
18	20	4.6	1.3
18	100	23	0.26

For the 2PDI at photon energy of 70 eV, the DSI peaks are located at energies

$$E_1^{\text{DSI}} = \omega_{\text{XUV}} - I_1 \quad (18)$$

and

$$E_2^{\text{DSI}} = \omega_{\text{XUV}} - I_2, \quad (19)$$

where $I_1 = 24.6$ and $I_2 = 54.4$ eV are the first and the second ionization potentials of helium, respectively.

For 3PDI at 35 eV, the two DSI peaks appear at

$$E_1^{\text{DSI}} = \omega_{\text{XUV}} - I_1 \quad (20)$$

and

$$E_2^{\text{DSI}} = 2\omega_{\text{XUV}} - I_2. \quad (21)$$

Note that in reverse order, the absorption of two photons in the first ionization step and one photon in the second ionization step cannot contribute to direct ionization since the one-photon energy of 35 eV lies below the second ionization potential. However, the excitation-ionization channel is open

with

$$E_1^{\text{EI-I}} = 2\omega_{\text{XUV}} - I_1 - (E_{2l} - E_{1s}) \quad (22)$$

and

$$E_2^{\text{EI-I}} = \omega_{\text{XUV}} + E_{2l}, \quad (23)$$

where E_{1s} is the ground-state energy and E_{2l} the $n = 2$ excited-state energies (l : angular momentum) of He^+ . The threshold for excitation ionization lies at $I_{p1} + (E_{2l} - E_{1s}) = 65.4$ eV. The key point to be noted is that the DSI and EI-I pathways lead to different joint energy distributions, marked by arrows in Fig. 2(c3), both lying on the circle with $k_1^2 + k_2^2 = \text{const}$. Remarkably, the intensities of the DSI and the EI-I contributions are of comparable magnitude. This is different from 2PDI with $\omega_{\text{XUV}} = 70$ eV where the EI-I pathway is also energetically open [104], but remains invisibly small [Fig. 2(a3)]. The yield of the first step of the EI-I pathway is much weaker in comparison with direct ionization in the DSI pathway, resulting in the suppression of the EI-I pathway. In the 3PDI at 35 eV, despite the fact that the yield of two-photon excitation ionization in the first step of the EI-I pathway is also much weaker than the direct one-photon ionization in the DSI pathway, in the second step the relative strength of the two pathways is reversed. Therefore, both channels have comparable strengths.

For 4PDI at 22 eV, the DSI path is energetically closed, while the EI-I path [Figs. 2(d3) and 2(d4)] is characterized by the energies

$$E_1^{\text{EI-I}} = 3\omega_{\text{XUV}} - I_{p1} - (E_{2l} - E_{1s}) \quad (24)$$

and

$$E_2^{\text{EI-I}} = \omega_{\text{XUV}} + E_{2l}. \quad (25)$$

For 5PDI with photon energies near 18 eV, different pathways are available: a multiphoton DSI path with

$$E_1^{\text{DSI}} = 2\omega_{\text{XUV}} - I_1 \quad (26)$$

and

$$E_2^{\text{DSI}} = 3\omega_{\text{XUV}} - I_2, \quad (27)$$

when the finite Fourier width of the pulse can close the small residual gap of 0.4 eV to the second ionization threshold [Eq. (27)], and the EI-I paths with

$$E_1^{\text{EI-I}} = 4\omega_{\text{XUV}} - I_{p1} - (E_{2l} - E_{1s}) \quad (28)$$

and

$$E_2^{\text{EI-I}} = \omega_{\text{XUV}} + E_{2l}. \quad (29)$$

For all MPDI processes, the dependence of the joint radial momentum spectra on T_p is qualitatively similar. As the pulse duration decreases to 20 cycles, the DSI and EI-I peaks display increased Fourier broadening. At even shorter pulse duration of $T_p = 5$ cycles, the separate peaks merge into a single peak at equal energy sharing, rendering the notion of sequentiality obsolete. Interestingly, in this ultrashort limit, Fourier broadening allows the $(n_{\text{ph}} - 1)$ PDI process to compete with, or even dominate over, the n_{ph} PDI channel (see the first row in Fig. 2).

B. Electron-electron correlation effects in the angle-resolved spectra

Electron-electron correlation can alter the angular distributions even for nominally sequential ionization due to the short interval between the two single-ionization (SI) steps. In particular, when the two electrons are ejected into the same direction, the repulsive electron-electron potential will force the two electrons to part ways. To reveal this dynamical correlation, we investigate angle-resolved two-electron energy spectra. The angle-resolved energy spectrum in the $x - z$ plane (with $\phi_1 = \phi_2 = 0$) is defined by

$$P(E_1, \theta_{12}) = \int P(k_1, \Omega_1, k_2, \Omega_2) k_1 k_2^2 dk_2, \quad (30)$$

with the ejection direction of one electron fixed at $\theta_1 = 0$. Previous results limited to 2PDI can be found in Ref. [67].

The feature common to all orders of MPDI for the shortest $T_p = 5$ cycles [Figs. 3(a1), 3(b1), 3(c1), and 3(d1)] is the suppression of equal-energy ionization at a relative angle $\theta_{12} = 0$, as result of strong Coulomb repulsion. By contrast, for longer pulse durations, ionization peaks can be found both at $\theta_{12} = 0$ as well as $\theta_{12} = 180^\circ$ for most of the sequential MPDI processes in Fig. 3. One interesting case is the 3PDI [Figs. 3(c2) and 3(c3)] for which both the DSI and the EI-I processes contribute and both can be clearly identified at $\theta_{12} = 180^\circ$. For small θ_{12} , however, unexpected structures appear that can be identified as signatures of dynamical correlations in the exit channel at remarkably large distances from the nucleus. The origin of this ‘‘postcollision’’ electron-electron interaction lies in the particular kinematics of the two-electron emission in 3PDI at this photon energy ($\hbar\omega = 35$ eV). In both the DSI and the EI-I processes, the first of the sequentially emitted electrons has a smaller velocity than the second (DSI: $v_1 = 0.87$, $v_2 = 1.07$; EI-I: $v_1 = 0.58$, $v_2 = 1.25$). When these initially only weakly correlated electrons are emitted into nearly the same direction, the second electron will catch up with the first and, eventually, a quasifree electron-electron scattering event will ensue. As the time spacing between sequential emission is of the order of $T_p/2$, for longer pulses the resulting collision time for e-e scattering $t_c = v_1 T_p / 2(v_2 - v_1)$ becomes very large, e.g., for the 20 cycle pulse and for DSI $t_c \approx 220$ a.u. At this instance, the distance of the receding electrons from the He^{2+} ion is already $d_c \approx 240$ a.u. Moreover, scattering at such large distances involves large single-particle angular momenta $l_{1,2}$ (see also Fig. 5). Extending the full quantum simulation based on the atomic TDCC expansion [Eq. (4)] to such large distances, long interactions times, and high angular momenta poses a considerable numerical challenge.

To analyze the data and to probe for convergence, we therefore perform, in parallel, CTMC simulations. The latter also allow one to simulate the asymptotic $E - \theta_{12}$ distribution for the longest pulse (100 cycles) for which fully converged quantum simulations are currently out of reach. The comparison between the quantum and classical $E - \theta_{12}$ distributions for emission into the same hemisphere ($\theta_{12} < 90^\circ$) by the 20-cycle pulse [Figs. 4(a)–4(c)] with propagation up to time $t_{\text{max}} = 500$ a.u. displays close structural similarities. In particular, the ‘‘hole’’ in the distributions near $\theta_{12} = 0$ centered at equal-energy sharing $(E_1 + E_2)/2$ signifies the Newton circle

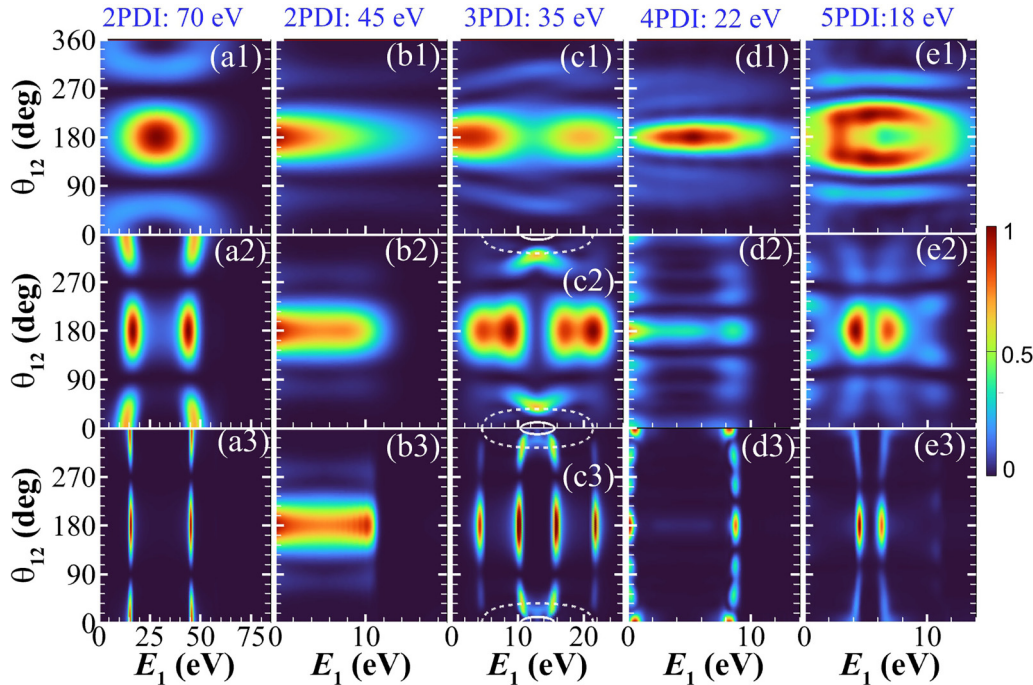


FIG. 3. For the same MPDI processes as in Fig. 2, the angle-resolved energy spectra $P(E_1, \theta_{12})$ at $\theta_1 = 0$ [see Eq. (30)]. The contributions of $(n_{\text{ph}} - 1)$ PDI at five cycles are omitted for clarity by restricting the integral in Eq. (30) to the region $k_1^2 + k_2^2 > k_c^2$, with k_c the lower cutoff momentum chosen as 1.2, 1.0, 0.5, and 0.65 a.u. for photon energies 70, 35, 22, and 18 eV, respectively. In (c2) and (c3), the Newton circles for quasifree electron-electron (e-e) scattering, mapped onto the $E - \theta_{12}$ plane, are shown. Note that (c3) represents a snapshot at $t_{\text{max}} = 500$ a.u., rather than the asymptotic distribution (for details, see text). We use relative decimal color scale values. Absolute total probabilities are given in Fig. 2.

of quasifree e-e scattering in the weak ionic Coulomb field [also indicated in Figs. 3(c2) and 3(c3)], given by

$$E_1 = \frac{1}{2}(E_1^C + E_2^C) - \frac{1}{2}(E_2^C - E_1^C) \cos \alpha, \quad (31)$$

$$\theta_{12} = \tan^{-1} \left[\frac{(v_2 - v_1) \sin \alpha}{(v_1 + v_2) + (v_2 - v_1) \cos \alpha} + \frac{(v_2 - v_1) \sin \alpha}{(v_1 + v_2) - (v_2 - v_1) \cos \alpha} \right], \quad (32)$$

where α is the scattering angle in the center-of-mass frame of the two electrons, E_i^C ($C = \text{DSI}$ or EI-I) are energies of the electrons given by Eqs. (20)–(23) for strictly sequential and uncorrelated emission, and $v_i = \sqrt{2E_i^C}$.

Further propagation of the classical ensemble [Fig. 4(c)] beyond the time interval subtended by the quantal simulation [Figs. 4(a) and 4(b)] leaves the $E - \theta_{12}$ distribution largely unchanged, thereby indicating its convergence. For the longer 100-cycle pulse [Figs. 4(d) and 4(f)], the quantum simulation of the $E - \theta_{12}$ distribution [Fig. 3(c3), magnified in Fig. 4(d)] can provide only a snapshot of the distribution taken at $t_{\text{max}} = 500$ a.u., which resembles the corresponding classical distribution extracted at this time [Fig. 4(e)]. Remarkably, the Newton circle of the EI-I channel can be identified for the 100-cycle pulse in Fig. 4(d), though e-e scattering in the DSI channel has not yet fully converged. The fact that the observed holes in Figs. 4 and 5 have somewhat larger radii than the Newton circles predicted by the analytical estimate

[Eqs. (31) and (32)], in particular for the shorter 20-cycle pulse, signifies the influence of the residual Coulomb field of the nucleus on the e-e scattering process. Most importantly, the local velocities of the electrons at the instant of

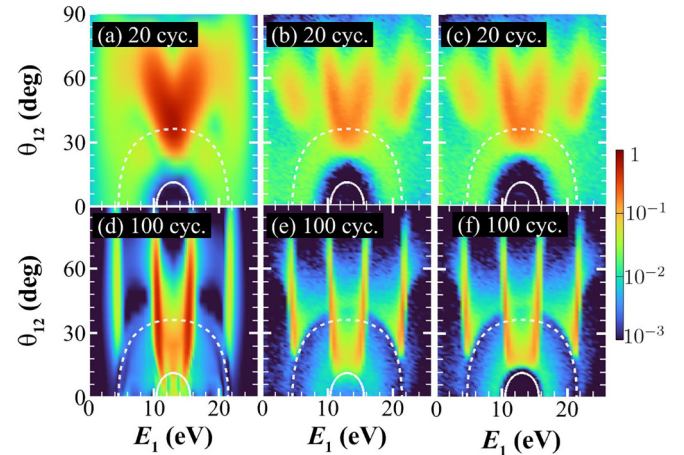


FIG. 4. $P(E_1, \theta_{12})$ distributions for 3PDI (logarithmic color scales are used for visibility) for emission into the same hemisphere ($\theta_{12} < 90^\circ$). (a)–(c) 20 cycle pulse, with (a) quantum and (b) classical distribution, each extracted at $t_{\text{max}} = 500$ a.u., and (c) asymptotic ($t_{\text{max}} \rightarrow \infty$) classical distribution. (d)–(f) 100-cycle pulse, with (d) quantum and (e) classical distribution, each extracted at $t_{\text{max}} = 500$ a.u., and (f) asymptotic ($t_{\text{max}} \rightarrow \infty$) classical distribution. Solid (dashed) white lines represent the Newton circle for DSI (EI-I) electrons.

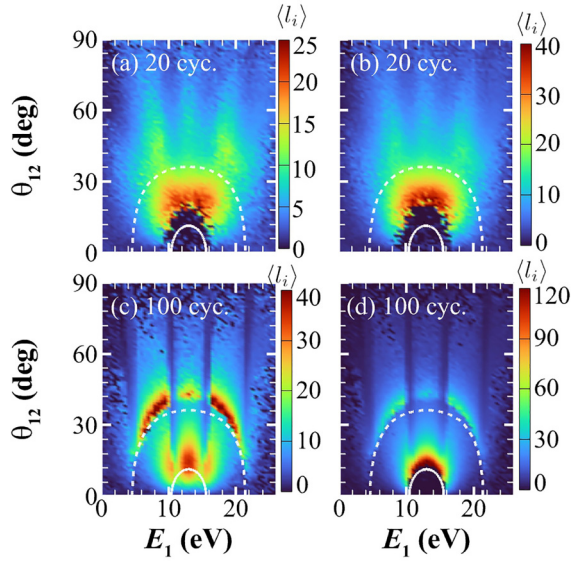


FIG. 5. Mean single-particle angular momentum $\langle l_i \rangle$ ($i = 1, 2$) contributions to the classical $P(E, \theta_{12})$ distributions (see Fig. 4) for 3PDI and pulse durations of 20 cycles (a), (b) and 100 cycles (c), (d). Both (a), (c) snapshot at $t_{\max} = 500$ a.u. and (b), (d) asymptotic distributions are shown.

scattering are larger than the asymptotic velocities entering Eqs. (31) and (32). Inside the Newton circle of DSI (the solid line in each panel), the asymptotic stationary $E - \theta_{12}$ distribution ($t \rightarrow \infty$) [Fig. 4(f)] is reached only much later and still differs from the snapshots at t_{\max} [Fig. 4(e)]. The reason is that at t_{\max} , the DSI scattering process has not yet

concluded. This e-e scattering resulting from the “catching up” of the faster second electron with the slower first electron at late times t_c and large distances d_c from the nucleus also has remarkable consequences for the single-particle angular momentum distributions of the electrons in the exit channel (Fig. 5). The classical angular momentum transfer between the electrons extends to the order of $l_i \approx |\mathbf{d}_c \times (\mathbf{v}_2 - \mathbf{v}_1)|$, as seen in the frame of the nucleus. (Of course, the total angular momentum L remains conserved and small as it is controlled by the number of absorbed photons). As expected, the distribution of mean single-electron angular momenta $\langle l_i \rangle$ peaks near the Newton circle. This $\langle l_i \rangle$ distribution illustrates the challenge this postcollision e-e scattering process poses for quantum simulations based on atom-centered spherical harmonics expansions [Eq. (4)].

We note that the present catching-up correlation dynamics resembles the postcollision interaction between direct slow and fast Auger electron emission [105,106]. The present MPDI-induced scattering differs from the Auger electron scattering in that the velocity difference between the two electrons is rather small and the temporal spacing is controlled by the pulse shape, resulting in quasifree electron-electron scattering at very large distances from the ion.

The pulse-duration controlled electron-electron correlation effects can also be clearly identified by further integrating $P(E_1, \theta_{12})$ over the energy E_1 ,

$$P(\theta_{12}) = \int P(E_1, \theta_{12}) dE_1. \quad (33)$$

The resulting equal-intensity lines for the conditional angular distributions $P(\theta_{12})$ are shown in Fig. 6, where the suppression of the ejection along the same direction for short T_p is visible

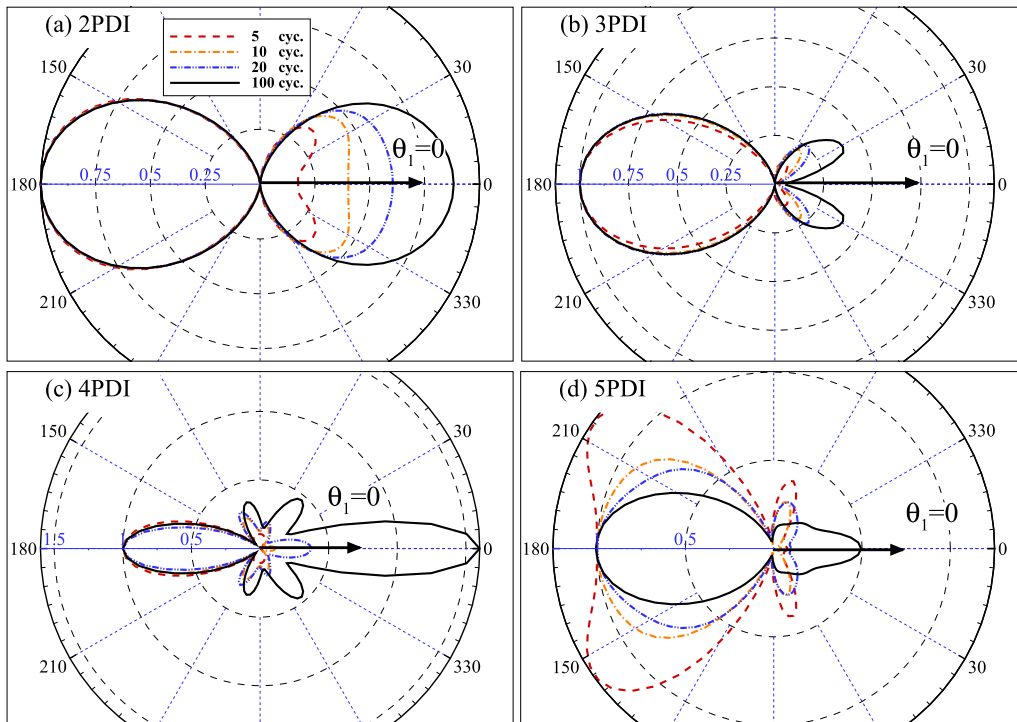


FIG. 6. For the same MPDI processes as in Fig. 2, the conditional angular distributions $P(\theta_{12})$ at $\theta_1 = 0$ [Eq. (33)] of the ejected electrons for different pulse durations for (a) 2PDI at 70 eV, (b) 3PDI at 35 eV, (c) 4PDI at 22 eV, and (d) 5PDI at 18 eV.

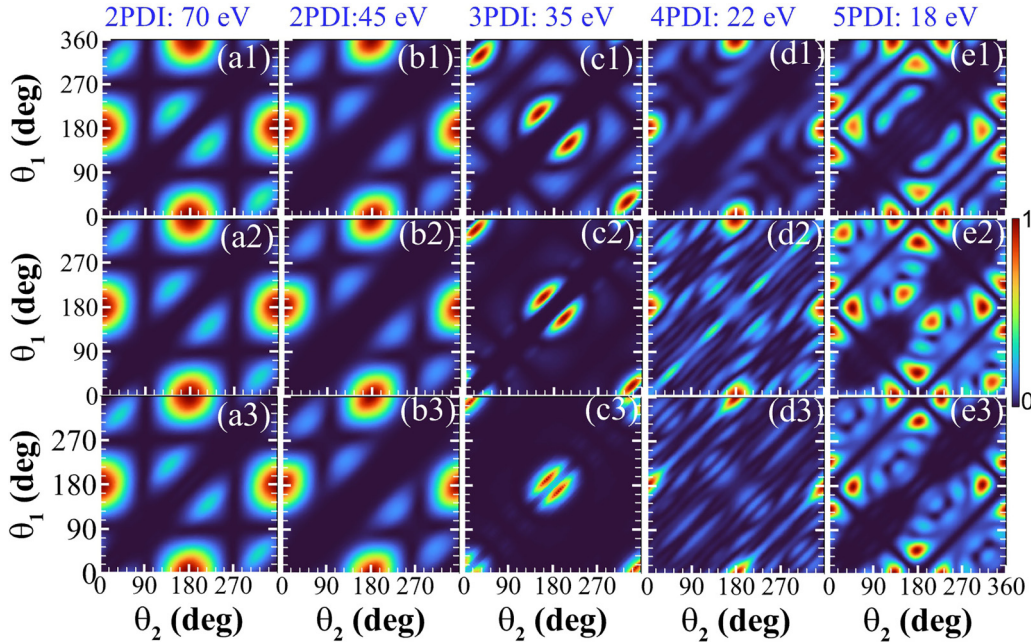


FIG. 7. For the same MPDI processes as in Fig. 2, the coplanar angular distributions ($\phi_1 = \phi_2 = 0$) at equal photoelectron energies, $E_1 = E_2 = n_{\text{ph}}\omega_{\text{XUV}} - I_p$. Note that (c3) represents a snapshot at $t_{\text{max}} = 500$ a.u. rather than the converged asymptotic distribution (see text).

for all MPDI. We note that the variation of conditional angular distributions with T_p is particularly strong for 5PDI, not only near $\theta_{12} = 0$, but also for back-to-back emission, $\theta_{12} \leq 180^\circ$.

One frequently discussed selection rule in 1PDI is the vanishing equal-energy back-to-back ejection as a result of the parity-selection rule. As this selection rule is only determined by the parity of the final two-electron continuum state [5,107], it applies to all MPDI processes when an odd number of photons is involved [85,107]. Therefore, the equal-energy back-to-back ejection in MPDI is alternately suppressed or enhanced when the photon number is increased by one. This selection rule also leaves its mark on the angular differential energy spectra $P(E_1, \theta_{12})$ (Fig. 3). The SI peaks at $\theta_{12} = 180^\circ$ merge into a single peak at equal energies for 2PDI and 4PDI, but this is not the case for 3PDI and 5PDI. Its influence is even more clearly demonstrated in Fig. 7, where the equal-energy joint angular distributions in the $x-z$ plane are shown. The most dominant ejection mode for 2PDI and 4PDI is the back-to-back emission, with one electron ejected along $\theta = 0$ and the other along $\theta = 180^\circ$, while this mode is strictly forbidden for 3PDI and 5PDI.

The influence of the pulse duration T_p on the equal-energy distribution strongly varies with the order of the process. For 2PDI, its influence is nearly negligible. While for 4PDI and 5PDI the dominant ejection direction remains unchanged, the intensity ratios relative to other directions vary significantly. For 3PDI, we observe, for larger T_p , features of e-e scattering when both electrons are emitted near the forward ($\theta_1 = \theta_2 = 0$) or the backward ($\theta_1 = \theta_2 = 180^\circ$) direction [Figs. 7(c2) and 7(c3)]. For $T_p = 20$ cycles, the joint distribution has converged [Fig. 7(c2)], while for the longest pulse [Fig. 7(c3)], the e-e scattering has not yet concluded and Fig. 7(c3) should be viewed as a snapshot at $t_{\text{max}} = 500$ a.u. We note that a strong same-direction ejection mode was previously seen

in the equal-energy coplanar distribution for 3PDI at 42 eV [36]. This could possibly also be an indication of incomplete convergence due to e-e scattering at large distances.

To illustrate the influence of the pulse duration in more detail, we display, in Fig. 8, equal-intensity lines for the cut through the joint angular distribution (Fig. 7) at $\theta_1 = 0$. The comparison between Fig. 8 and Fig. 6 highlights that side-by-side emission is suppressed when restricting the spectra to equal-energy sharing. 3PDI provides the remarkable exception where side-by-side emission dominates for the longer pulses as a result of the e-e scattering. As can be seen in Figs. 3(a)–3(c), the e-e scattering can indeed result in equal-energy ejection with small angle, located near the Newton circles.

C. The joint momentum distribution along the laser polarization

Several previous studies of strong-IR field DI have focused on the joint momentum distributions along the laser polarization axis [21–27,29], often also referred to as momentum correlation. For 2PDI, results were presented in Ref. [108]. The joint momentum distribution along the laser polarization z axis is defined as

$$P(k_{1z}, k_{2z}) = \int P(\mathbf{k}_1, \mathbf{k}_2) dk_{1x} dk_{1y} dk_{2x} dk_{2y}. \quad (34)$$

Exploiting the azimuthal symmetry of Eq. (14), Eq. (34) can be reduced to a triple integral,

$$P(k_{1z}, k_{2z}) = 2\pi \int_{|k_{2z}|}^{\infty} \int_{|k_{1z}|}^{\infty} \int_0^{2\pi} k_1 k_2 P\left(k_1, \arccos \frac{k_{1z}}{k_1}, 0, k_2, \arccos \frac{k_{2z}}{k_2}, \Delta\phi\right) d\Delta\phi dk_1 dk_2, \quad (35)$$

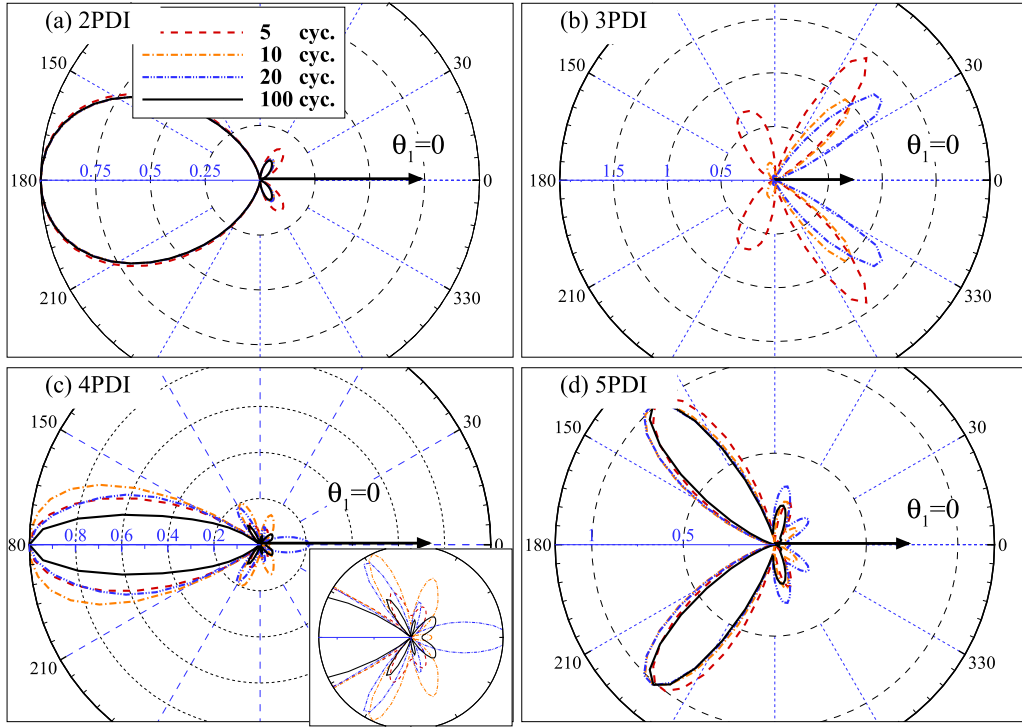


FIG. 8. Normalized conditional angular distributions $P(\theta_{12}, \theta_1 = 0, E_1 = E_2)$ at equal energies of two photoelectrons, $E_1 = E_2 = n_{\text{ph}}\omega - I_p$ (cuts through Fig. 7 at $\theta_1 = 0$), similar to Fig. 6 but restricted to equal energy sharing.

with $\Delta\phi = \phi_2 - \phi_1$ the difference between the azimuthal angles of the two emitted electrons. In the correlated momentum spectra (Fig. 9), the exchange symmetry of the two electrons is reflected in the symmetry relative to the line $k_{1z} = k_{2z}$. In Fig. 9, we can also observe another, approximate symmetry relative to the line $k_{1z} = -k_{2z}$. This symmetry,

however, holds only for long constant amplitude pulses when carrier-envelope phase (CEP) effects are negligible. In this limit, the ejection along the positive and negative laser polarization directions has exactly the same probability. Its breakdown for ultrashort pulses can be clearly seen, e.g., in Fig. 9(d1).

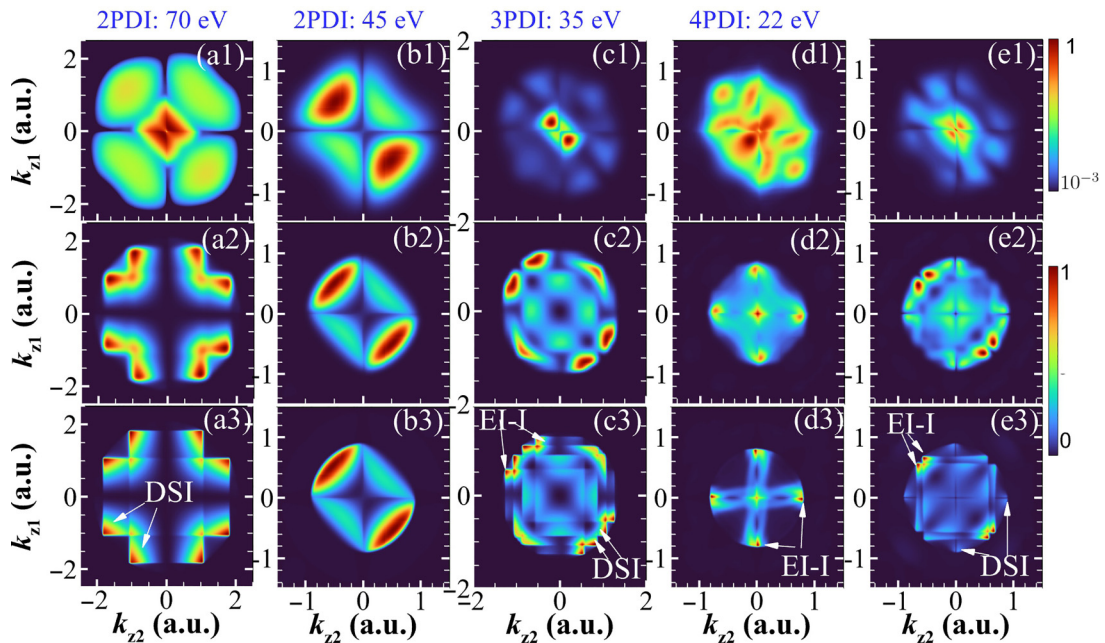


FIG. 9. For the same MPDI processes as in Fig. 2, the joint momentum distribution along the laser polarization axis $P(k_{z1}, k_{z2})$ [Eq. (34)]. Note that (unlike for the other frames) we use a logarithmic color scale in (a1) to render the 2PDI process relative to the 1PDI visible.

The emerging momentum correlation patterns are frequently characterized by the dominance of either “correlated emission” (i.e., $k_{z1}k_{z2} > 0$, corresponding to preferred emission into the first or third quadrant in the $k_{1z} - k_{2z}$ plane; see Fig. 9) or “anticorrelated emission” (i.e., $k_{z1}k_{z2} < 0$, preferred emission into the second or fourth quadrant). Our present results show that such preferences strongly depend both on the order of the multiphoton process and on the pulse duration. While for nonsequential 2PDI at photon energies below $\omega_{XUV} = I_2$, anticorrelated ejection dominates [108], for sequential 2PDI at $\omega_{XUV} = 70$ eV, no clear preference for either correlated or anticorrelated emission emerges, with the exception for the shortest pulse, $T_p = 5$ cycles, where the backward-forward symmetry is obviously broken for the 2PDI and the 1PDI signals at low momentum prefer the side-by-side ejection mode. For 3PDI, dominant anticorrelation prevails for all T_p , while for 5PDI, this trend is only pronounced for $T_p \geq 20$ cycles. For 4PDI, where only the EI-I channel is open for sequential ionization, no clear correlation or anticorrelation pattern emerges for $T_p \geq 20$ cycles. For the shortest pulse [Fig. 9(d1)], a complex pattern with slight preference for positive correlation appears which reflects the temporal nonsequentiality and the contribution from the $(n_{\text{ph}} - 1)$ PDI channel.

V. CONCLUDING REMARKS

In this work, we have systematically investigated double ionization of helium by ultrashort XUV pulses by varying the number of absorbed photons (up to five) and the pulse duration from about 100 attoseconds to 20 femtoseconds. We have explored the interplay between sequential and nonsequential double ionization for different photon orders and have identified alternative pathways towards double ionization. Most importantly, we find that a path involving a multiphoton

two-electron excitation-ionization step followed by a one- or multiphoton ionization of excited He^+ competes with the direct nonresonant sequential ionization via the ground state of He^+ . Electron correlation effects are also shown to be of importance for sequential processes. This applies to both the first step, where correlation effects are crucial in the two-electron transition leading to excitation ionization, as well as to the final state in the two-electron continuum, where the catching-up dynamics can lead to electron-electron scattering and energy exchange between the two electrons at large distances from the core. For ultrashort pulses in the attosecond regime, MPDI becomes strongly nonsequential with correlation effects in the time domain even in the spectrally sequential regime. Experimental observation of the processes delineated by the present *ab initio* TDSE simulation should be in reach of experiments employing the currently available strong XUV and X-laser pulses from free-electron laser sources.

ACKNOWLEDGMENTS

This work is supported by the National Natural Science Foundation of China (NSFC) (Grant No. 12074265), the Guangdong Basic and Applied Basic Research Foundation (Grant No. 2022A1515010329), the Austrian Science Fund (FWF) (Grant No. P35539-N), the International Max Planck Research School for Advanced Photon Science (APS), Grants No. FWF-SFB041-VICOM (Austria), No. FWF-SFB049-NEXTLITE (Austria), and No. FWF-W1243-SOLIDS4FUN (Austria), WWTF Grant No. MA-14002, COST Action CA18234, and COST Action AttoChem CA18222. J.F. acknowledges support by the Spanish Ministry for Science, Innovation, and Universities—Agencia Estatal de Investigación through Grants No. PID2021-125894NB-I00 and No. CEX2018-000805-M (through the María de Maeztu program for Units of Excellence in Research and Development).

-
- [1] W. Becker, X. J. Liu, P. J. Ho, and J. H. Eberly, Theories of photoelectron correlation in laser-driven multiple atomic ionization, *Rev. Mod. Phys.* **84**, 1011 (2012).
 - [2] L.-Y. Peng, W.-C. Jiang, J.-W. Geng, W.-H. Xiong, and Q. Gong, Tracing and controlling electronic dynamics in atoms and molecules by attosecond pulses, *Phys. Rep.* **575**, 1 (2015).
 - [3] J. S. Briggs and V. Schmidt, Differential cross sections for photo-double-ionization of the helium atom, *J. Phys. B* **33**, R1 (2000).
 - [4] L. Avaldi and A. Huetz, Photodouble ionization and the dynamics of electron pairs in the continuum, *J. Phys. B* **38**, S861 (2005).
 - [5] A. Huetz, P. Selles, D. Waymel, and J. Mazeau, Wannier theory for double photoionization of noble gases, *J. Phys. B* **24**, 1917 (1991).
 - [6] F. W. Byron and C. J. Joachain, Multiple ionization processes in helium, *Phys. Rev.* **164**, 1 (1967).
 - [7] T. Åberg, Asymptotic double-photoexcitation cross sections of the helium atom, *Phys. Rev. A* **2**, 1726 (1970).
 - [8] T. Pattard, T. Schneider, and J. M. Rost, On the role of shake-off in single-photon double ionization, *J. Phys. B* **36**, L189 (2003).
 - [9] A. S. Kheifets, Shake-off process in non-sequential single-photon double ionization of closed-shell atomic targets, *Atoms* **10**, 89 (2022).
 - [10] A. Dalgarno and H. R. Sadeghpour, Double photoionization of atomic helium and its isoelectronic partners at x-ray energies, *Phys. Rev. A* **46**, R3591(R) (1992).
 - [11] Y. Qiu, J.-Z. Tang, J. Burgdörfer, and J. Wang, Double photoionization of helium from threshold to high energies, *Phys. Rev. A* **57**, R1489(R) (1998).
 - [12] W.-C. Jiang, L.-Y. Peng, W.-H. Xiong, and Q. Gong, Comparison study of electron correlation in one-photon and two-photon double ionization of helium, *Phys. Rev. A* **88**, 023410 (2013).
 - [13] L. R. Andersson and J. Burgdörfer, Excitation Ionization and Double Ionization of Helium by High-Energy Photon Impact, *Phys. Rev. Lett.* **71**, 50 (1993).
 - [14] A. Y. Istomin, N. L. Manakov, A. V. Meremianin, and A. F. Starace, Nondipole Effects in Photo-Double-Ionization of He by a vuv Photon, *Phys. Rev. Lett.* **92**, 063002 (2004).
 - [15] M. S. Schöffler, C. Stuck, M. Waitz, F. Trinter, T. Jahnke, U. Lenz, M. Jones, A. Belkacem, A. L. Landers, M. S. Pindzola, C. L. Cocke, J. Colgan, A. Kheifets, I. Bray,

- H. Schmidt-Böcking, R. Dörner, and T. Weber, Ejection of Quasi-Free-Electron Pairs from the Helium-Atom Ground State by Single-Photon Absorption, *Phys. Rev. Lett.* **111**, 013003 (2013).
- [16] S.-G. Chen, W.-C. Jiang, S. Grundmann, F. Trinter, M. S. Schöffler, T. Jahnke, R. Dörner, H. Liang, M.-X. Wang, L.-Y. Peng, and Q. Gong, Photon Momentum Transfer in Single-Photon Double Ionization of Helium, *Phys. Rev. Lett.* **124**, 043201 (2020).
- [17] A. Hishikawa, M. Fushitani, Y. Hikosaka, A. Matsuda, C.-N. Liu, T. Morishita, E. Shigemasa, M. Nagasono, K. Tono, T. Togashi, H. Ohashi, H. Kimura, Y. Senba, M. Yabashi, and T. Ishikawa, Enhanced Nonlinear Double Excitation of He in Intense Extreme Ultraviolet Laser Fields, *Phys. Rev. Lett.* **107**, 243003 (2011).
- [18] B. Walker, B. Sheehy, L. F. DiMauro, P. Agostini, K. J. Schafer, and K. C. Kulander, Precision Measurement of Strong Field Double Ionization of Helium, *Phys. Rev. Lett.* **73**, 1227 (1994).
- [19] F. Mauger, C. Chandre, and T. Uzer, Recollisions and Correlated Double Ionization with Circularly Polarized Light, *Phys. Rev. Lett.* **105**, 083002 (2010).
- [20] F. Mauger, C. Chandre, and T. Uzer, From Recollisions to the Knee: A Road Map for Double Ionization in Intense Laser Fields, *Phys. Rev. Lett.* **104**, 043005 (2010).
- [21] T. Weber, H. Giessen, M. Weckenbrock, G. Urbasch, A. Staudte, L. Spielberger, O. Jagutzki, V. Mergel, M. Vollmer, and R. Dörner, Correlated electron emission in multiphoton double ionization, *Nature (London)* **405**, 658 (2000).
- [22] A. Rudenko, V. L. B. de Jesus, T. Ergler, K. Zrost, B. Feuerstein, C. D. Schröter, R. Moshhammer, and J. Ullrich, Correlated Two-Electron Momentum Spectra for Strong-Field Nonsequential Double Ionization of He at 800 nm, *Phys. Rev. Lett.* **99**, 263003 (2007).
- [23] X. Sun, M. Li, D. Ye, G. Xin, L. Fu, X. Xie, Y. Deng, C. Wu, J. Liu, Q. Gong, and Y. Liu, Mechanisms of Strong-Field Double Ionization of Xe, *Phys. Rev. Lett.* **113**, 103001 (2014).
- [24] A. Staudte, C. Ruiz, M. Schöffler, S. Schössler, D. Zeidler, T. Weber, M. Meckel, D. M. Villeneuve, P. B. Corkum, A. Becker, and R. Dörner, Binary and Recoil Collisions in Strong Field Double Ionization of Helium, *Phys. Rev. Lett.* **99**, 263002 (2007).
- [25] B. Bergues, M. Kuebel, N. G. Johnson, B. Fischer, N. Camus, K. J. Betsch, O. Herrwerth, A. Senftleben, A. M. Saylor, T. Rathje, T. Pfeifer, I. Ben-Itzhak, R. R. Jones, G. G. Paulus, F. Krausz, R. Moshhammer, J. Ullrich, and M. F. Kling, Attosecond tracing of correlated electron-emission in non-sequential double ionization, *Nat. Commun.* **3**, 813 (2012).
- [26] Y. Liu, S. Tschuch, A. Rudenko, M. Dürr, M. Siegel, U. Morgner, R. Moshhammer, and J. Ullrich, Strong-Field Double Ionization of Ar below the Recollision Threshold, *Phys. Rev. Lett.* **101**, 053001 (2008).
- [27] B. Wolter, M. G. Pullen, M. Baudisch, M. Sclafani, M. Hemmer, A. Senftleben, C. D. Schröter, J. Ullrich, R. Moshhammer, and J. Biegert, Strong-Field Physics with Mid-IR Fields, *Phys. Rev. X* **5**, 021034 (2015).
- [28] P. B. Corkum, Plasma Perspective on Strong Field Multiphoton Ionization, *Phys. Rev. Lett.* **71**, 1994 (1993).
- [29] Z. Chen, S. Li, H. Kang, T. Morishita, and K. Bartschat, Ellipticity dependence of anticorrelation in the nonsequential double ionization of ar, *Opt. Express* **30**, 44039 (2022).
- [30] Z. Yuan, D. Ye, J. Liu, and L. Fu, Inner-shell electron effects in strong-field double ionization of xe, *Phys. Rev. A* **93**, 063409 (2016).
- [31] J. S. Prauzner-Bechcicki, K. Sacha, B. Eckhardt, and J. Zakrzewski, Time-Resolved Quantum Dynamics of Double Ionization in Strong Laser Fields, *Phys. Rev. Lett.* **98**, 203002 (2007).
- [32] C. Huang, M. Zhong, and Z. Wu, Recollision dynamics in nonsequential double ionization of atoms by long-wavelength pulses, *Opt. Express* **24**, 28361 (2016).
- [33] X. L. Hao, J. Chen, W. D. Li, B. Wang, X. Wang, and W. Becker, Quantum Effects in Double Ionization of Argon below the Threshold Intensity, *Phys. Rev. Lett.* **112**, 073002 (2014).
- [34] J. Su, Z. Liu, J. Liao, X. Huang, Y. Li, and C. Huang, Electron correlation and recollision dynamics in nonsequential double ionization by counter-rotating two-color elliptically polarized laser fields, *Opt. Express* **30**, 24898 (2022).
- [35] S. X. Hu, Boosting Photoabsorption by Attosecond Control of Electron Correlation, *Phys. Rev. Lett.* **111**, 123003 (2013).
- [36] A. Zielinski, V. P. Majety, and A. Scrinzi, Double photoelectron momentum spectra of helium at infrared wavelength, *Phys. Rev. A* **93**, 023406 (2016).
- [37] M. Kurka, J. Feist, D. A. Horner, A. Rudenko, Y. H. Jiang, K. U. Kühnel, L. Foucar, T. N. Rescigno, C. W. McCurdy, R. Pazourek, S. Nagele, M. Schulz, O. Herrwerth, M. Lezius, M. F. Kling, M. Schöffler, A. Belkacem, S. Düsterer, R. Treusch, B. I. Schneider *et al.*, Differential cross sections for non-sequential double ionization of he by 52 eV photons from the free electron laser in hamburg, flash, *New J. Phys.* **12**, 073035 (2010).
- [38] A. Rudenko, L. Foucar, M. Kurka, T. Ergler, K. U. Kühnel, Y. H. Jiang, A. Voitkiv, B. Najjari, A. Kheifets, S. Lüdemann, T. Havermeier, M. Smolarski, S. Schössler, K. Cole, M. Schöffler, R. Dörner, S. Düsterer, W. Li, B. Keitel, R. Treusch *et al.*, Recoil-Ion Momentum Distributions for Two-Photon Double Ionization of He and Ne by 44 eV Free-Electron Laser Radiation, *Phys. Rev. Lett.* **101**, 073003 (2008).
- [39] A. A. Sorokin, M. Wellhöfer, S. V. Bobashev, K. Tiedtke, and M. Richter, X-ray-laser interaction with matter and the role of multiphoton ionization: Free-electron-laser studies on neon and helium, *Phys. Rev. A* **75**, 051402(R) (2007).
- [40] Y. Nabekawa, H. Hasegawa, E. J. Takahashi, and K. Midorikawa, Production of Doubly Charged Helium Ions by Two-Photon Absorption of an Intense Sub-10-fs Soft X-Ray Pulse at 42 eV Photon Energy, *Phys. Rev. Lett.* **94**, 043001 (2005).
- [41] H. Hasegawa, E. J. Takahashi, Y. Nabekawa, K. L. Ishikawa, and K. Midorikawa, Multiphoton ionization of He by using intense high-order harmonics in the soft-x-ray region, *Phys. Rev. A* **71**, 023407 (2005).
- [42] B. Manschwetus, L. Rading, F. Campi, S. Maclot, H. Coudert-Alteirac, J. Lahl, H. Wikmark, P. Rudawski, C. M. Heyl, B. Farkas, T. Mohamed, A. L'Huillier, and P. Johnsson, Two-photon double ionization of neon using an intense attosecond pulse train, *Phys. Rev. A* **93**, 061402(R) (2016).
- [43] K. L. Ishikawa and K. Midorikawa, Above-threshold double ionization of helium with attosecond intense soft x-ray pulses, *Phys. Rev. A* **72**, 013407 (2005).

- [44] E. Fomoup, H. Bachau, and B. Piraux, $(2\gamma, 2e)$ total and differential cross-section calculations for helium with $\omega = 40\text{--}50$ eV, *Eur. Phys. J. Spec. Top.* **175**, 175 (2009).
- [45] X. Guan, K. Bartschat, and B. I. Schneider, Dynamics of two-photon double ionization of helium in short intense XUV laser pulses, *Phys. Rev. A* **77**, 043421 (2008).
- [46] S. X. Hu, J. Colgan, and L. A. Collins, Triple-differential cross-sections for two-photon double ionization of he near threshold, *J. Phys. B: At., Mol. Opt. Phys.* **38**, L35 (2005).
- [47] K. Stefańska, F. Reynal, and H. Bachau, Two-photon double ionization of $\text{He}(1s^2)$ and $\text{He}(1s2s\ ^1S)$ by XUV short pulses, *Phys. Rev. A* **85**, 053405 (2012).
- [48] D. A. Horner, F. Morales, T. N. Rescigno, F. Martín, and C. W. McCurdy, Two-photon double ionization of helium above and below the threshold for sequential ionization, *Phys. Rev. A* **76**, 030701(R) (2007).
- [49] D. A. Horner, C. W. McCurdy, and T. N. Rescigno, Triple differential cross sections and nuclear recoil in two-photon double ionization of helium, *Phys. Rev. A* **78**, 043416 (2008).
- [50] D. A. Horner, T. N. Rescigno, and C. W. McCurdy, Nuclear recoil cross sections from time-dependent studies of two-photon double ionization of helium, *Phys. Rev. A* **81**, 023410 (2010).
- [51] A. Palacios, T. N. Rescigno, and C. W. McCurdy, Time-dependent treatment of two-photon resonant single and double ionization of helium by ultrashort laser pulses, *Phys. Rev. A* **79**, 033402 (2009).
- [52] A. Palacios, D. A. Horner, T. N. Rescigno, and C. W. McCurdy, Two-photon double ionization of the helium atom by ultrashort pulses, *J. Phys. B: At., Mol. Opt. Phys.* **43**, 194003 (2010).
- [53] R. Shakeshaft, Two-photon single and double ionization of helium, *Phys. Rev. A* **76**, 063405 (2007).
- [54] H. Bachau, Theory of two-photon double ionization of helium at the sequential threshold, *Phys. Rev. A* **83**, 033403 (2011).
- [55] J. Feist, S. Nagele, R. Pazourek, E. Persson, B. I. Schneider, L. A. Collins, and J. Burgdörfer, Nonsequential two-photon double ionization of helium, *Phys. Rev. A* **77**, 043420 (2008).
- [56] R. Pazourek, J. Feist, S. Nagele, E. Persson, B. I. Schneider, L. A. Collins, and J. Burgdörfer, Universal features in sequential and nonsequential two-photon double ionization of helium, *Phys. Rev. A* **83**, 053418 (2011).
- [57] P. Lambropoulos, L. A. A. Nikolopoulos, M. G. Makris, and A. Mihelič, Direct versus sequential double ionization in atomic systems, *Phys. Rev. A* **78**, 055402 (2008).
- [58] J. Colgan and M. S. Pindzola, Core-Excited Resonance Enhancement in the Two-Photon Complete Fragmentation of Helium, *Phys. Rev. Lett.* **88**, 173002 (2002).
- [59] M. A. Kornberg and P. Lambropoulos, Photoelectron energy spectrum in 'direct' two-photon double ionization of helium, *J. Phys. B* **32**, L603 (1999).
- [60] L. Malegat, H. Bachau, B. Piraux, and F. Reynal, A novel estimate of the two-photon double-ionization cross section of helium, *J. Phys. B* **45**, 175601 (2012).
- [61] O. Chuluunbaatar, H. Bachau, Y. V. Popov, B. Piraux, and K. Stefańska, Two-photon double ionization of atoms in attosecond x-ray radiation fields, *Phys. Rev. A* **81**, 063424 (2010).
- [62] I. A. Ivanov and A. S. Kheifets, Angular anisotropy parameters for sequential two-photon double ionization of helium, *Phys. Rev. A* **79**, 023409 (2009).
- [63] P. Lambropoulos and L. A. A. Nikolopoulos, Angular distributions in double ionization of helium under xuv sub-femtosecond radiation, *New J. Phys.* **10**, 025012 (2008).
- [64] E. Fomouo, P. Antoine, H. Bachau, and B. Piraux, Attosecond timescale analysis of the dynamics of two-photon double ionization of helium, *New J. Phys.* **10**, 025017 (2008).
- [65] H. Bachau, E. Fomouo, P. Antoine, B. Piraux, O. Chuluunbaatar, Y. Popov, and R. Shakeshaft, Multiple ionization of atoms with XUV attosecond pulses: Two-photon double ionization of helium with 50 eV photons, *J. Phys.: Conf. Ser.* **212**, 012001 (2010).
- [66] E. Fomouo, G. L. Kamta, G. Edah, and B. Piraux, Theory of multiphoton single and double ionization of two-electron atomic systems driven by short-wavelength electric fields: An *ab initio* treatment, *Phys. Rev. A* **74**, 063409 (2006).
- [67] J. Feist, S. Nagele, R. Pazourek, E. Persson, B. I. Schneider, L. A. Collins, and J. Burgdörfer, Probing Electron Correlation via Attosecond XUV Pulses in the Two-Photon Double Ionization of Helium, *Phys. Rev. Lett.* **103**, 063002 (2009).
- [68] E. Fomouo, P. Antoine, B. Piraux, L. Malegat, H. Bachau, and R. Shakeshaft, Evidence for highly correlated electron dynamics in two-photon double ionization of helium, *J. Phys. B* **41**, 051001 (2008).
- [69] H. Bachau and P. Lambropoulos, Theory of the photoelectron spectrum in double ionization through two-photon absorption from $\text{He}(2s^2)$, *Phys. Rev. A* **44**, R9(R) (1991).
- [70] S. Laulan and H. Bachau, Correlation effects in two-photon single and double ionization of helium, *Phys. Rev. A* **68**, 013409 (2003).
- [71] S. Askeland, R. Nepstad, and M. Førre, Two-photon double ionization of helium by attosecond laser pulses: Evidence of highly correlated electron motion, *Phys. Rev. A* **85**, 035404 (2012).
- [72] S. Fritzsche, A. N. Grum-Grzhimailo, E. V. Gryzlova, and N. M. Kabachnik, Angular distributions and angular correlations in sequential two-photon double ionization of atoms, *J. Phys. B* **41**, 165601 (2008).
- [73] M. Førre, S. Selstø, and R. Nepstad, Nonsequential Two-Photon Double Ionization of Atoms: Identifying the Mechanism, *Phys. Rev. Lett.* **105**, 163001 (2010).
- [74] W.-C. Jiang, J.-Y. Shan, Q. Gong, and L.-Y. Peng, Virtual Sequential Picture for Nonsequential Two-Photon Double Ionization of Helium, *Phys. Rev. Lett.* **115**, 153002 (2015).
- [75] W.-C. Jiang, W.-H. Xiong, T.-S. Zhu, L.-Y. Peng, and Q. Gong, Double ionization of he by time-delayed attosecond pulses, *J. Phys. B* **47**, 091001 (2014).
- [76] Y. Tong, W.-C. Jiang, P. Wu, and L.-Y. Peng, Two-photon double ionization of helium by chirped few-cycle attosecond pulses: From nonsequential to sequential regime, *Chin. Phys. B* **25**, 073202 (2016).
- [77] W.-C. Jiang, Y. Tong, Q. Gong, and L.-Y. Peng, Recoil-momentum spectrum for few-photon double ionization of helium, *Phys. Rev. A* **89**, 043422 (2014).
- [78] C. Yu and L. B. Madsen, Sequential and nonsequential double ionization of helium by intense xuv laser pulses: Revealing ac stark shifts from joint energy spectra, *Phys. Rev. A* **94**, 053424 (2016).

- [79] S. Selstø, X. Raynaud, A. S. Simonsen, and M. Førre, Distinction between sequential and direct ionization in two-photon double ionization of helium, *Phys. Rev. A* **90**, 053412 (2014).
- [80] A. Liu and U. Thumm, Criterion for Distinguishing Sequential from Nonsequential Contributions to the Double Ionization of Helium in Ultrashort Extreme-Ultraviolet Pulses, *Phys. Rev. Lett.* **115**, 183002 (2015).
- [81] S. X. Hu, Electron-electron correlation in two-photon double ionization of he-like ions, *Phys. Rev. A* **97**, 013414 (2018).
- [82] M. S. Pindzola, G. M. Laurent, and J. P. Colgan, Multiphoton double ionization of helium using ultraviolet and infrared laser pulses, *J. Phys. B* **50**, 185601 (2017).
- [83] M. S. Pindzola, Y. Li, and J. Colgan, Multiphoton double ionization of helium using femtosecond laser pulses, *J. Phys. B* **49**, 215603 (2016).
- [84] A. Liu and U. Thumm, Laser-assisted XUV few-photon double ionization of helium: Joint angular distributions, *Phys. Rev. A* **89**, 063423 (2014).
- [85] H. Ni, S. Chen, C. Ruiz, and A. Becker, Selection rules in the few-photon double ionization of the helium atom, *J. Phys. B* **44**, 175601 (2011).
- [86] H. Ni, S. Chen, C. Ruiz, and A. Becker, Erratum: Selection rules in the few-photon double ionization of the helium atom, *J. Phys. B* **45**, 049601 (2012).
- [87] Z. Zhang, L.-Y. Peng, Q. Gong, and T. Morishita, Momentum space analysis of multiphoton double ionization of helium by intense attosecond XUV pulses, *Opt. Express* **18**, 8976 (2010).
- [88] H. Shimada, K. Komatsu, W. Komatsubara, T. Mizuno, S. Miyake, S. Minemoto, H. Sakai, T. Majima, S. Owada, T. Togashi, M. Yabashi, and A. Yagishita, Two- and three-photon double ionization of helium by soft x-ray free-electron laser pulses, *J. Phys. B* **52**, 065602 (2019).
- [89] Y. Hikosaka, M. Fushitani, A. Matsuda, T. Endo, Y. Toida, E. Shigemasa, M. Nagasono, K. Tono, T. Togashi, M. Yabashi, T. Ishikawa, and A. Hishikawa, Five-photon sequential double ionization of He in intense extreme-ultraviolet free-electron laser fields, *Phys. Rev. A* **90**, 053403 (2014).
- [90] Z. Zhang, L.-Y. Peng, M.-H. Xu, A. F. Starace, T. Morishita, and Q. Gong, Two-photon double ionization of helium: Evolution of the joint angular distribution with photon energy and two-electron energy sharing, *Phys. Rev. A* **84**, 043409 (2011).
- [91] T. N. Rescigno and C. W. McCurdy, Numerical grid methods for quantum-mechanical scattering problems, *Phys. Rev. A* **62**, 032706 (2000).
- [92] M. J. Rayson, Lagrange-Lobatto interpolating polynomials in the discrete variable representation, *Phys. Rev. E* **76**, 026704 (2007).
- [93] B. I. Schneider and L. A. Collins, The discrete variable method for the solution of the time-dependent Schrödinger equation, *J. Non-Cryst. Solids* **351**, 1551 (2005).
- [94] T. J. Park and J. C. Light, Unitary quantum time evolution by iterative Lanczos reduction, *J. Chem. Phys.* **85**, 5870 (1986).
- [95] E. S. Smyth, J. S. Parker, and K. Taylor, Numerical integration of the time-dependent Schrödinger equation for laser-driven helium, *Comput. Phys. Commun.* **114**, 1 (1998).
- [96] M. Hochbruck and C. Lubich, On Krylov subspace approximations to the matrix exponential operator, *SIAM J. Numer. Anal.* **34**, 1911 (1997).
- [97] B. I. Schneider, X. Guan, and K. Bartschat, Time propagation of partial differential equations using the short iterative Lanczos method and finite-element discrete variable representation, in *Concepts of Mathematical Physics in Chemistry: A Tribute to Frank E. Harris - Part B*, Advances in Quantum Chemistry, Vol. 72, edited by J. R. Sabin and R. Cabrera-Trujillo (Academic Press, San Diego, 2016), Chap. 5, pp. 95–127.
- [98] W.-C. Jiang and X.-Q. Tian, Efficient split-Lanczos propagator for strong-field ionization of atoms, *Opt. Express* **25**, 26832 (2017).
- [99] X. M. Tong, K. Hino, and N. Toshima, Phase-dependent atomic ionization in few-cycle intense laser fields, *Phys. Rev. A* **74**, 031405(R) (2006).
- [100] A. Scrinzi, Infinite-range exterior complex scaling as a perfect absorber in time-dependent problems, *Phys. Rev. A* **81**, 053845 (2010).
- [101] D. R. Schultz, L. Meng, and R. E. Olson, Classical description and calculation of ionization in collisions of 100 eV electrons and positrons with He and H₂, *J. Phys. B* **25**, 4601 (1992).
- [102] R. Abrines and I. C. Percival, Classical theory of charge transfer and ionization of hydrogen atoms by protons, *Proc. Phys. Soc.* **88**, 861 (1966).
- [103] K. I. Dimitriou, D. G. Arbó, S. Yoshida, E. Persson, and J. Burgdörfer, Origin of the double-peak structure in the momentum distribution of ionization of hydrogen atoms driven by strong laser fields, *Phys. Rev. A* **70**, 061401(R) (2004).
- [104] J. Feist, R. Pazourek, S. Nagele, E. Persson, B. I. Schneider, L. A. Collins, and J. Burgdörfer, Electron correlation in two-photon double ionization of helium from attosecond to XFEL pulses, *J. Phys. B* **42**, 134014 (2009).
- [105] A. L. Landers, F. Robicheaux, T. Jahnke, M. Schöffler, T. Osipov, J. Titze, S. Y. Lee, H. Adaniya, M. Hertlein, P. Ranitovic, I. Bocharova, D. Akoury, A. Bhandary, T. Weber, M. H. Prior, C. L. Cocke, R. Dörner, and A. Belkacem, Angular Correlation between Photoelectrons and Auger Electrons from *k*-Shell Ionization of Neon, *Phys. Rev. Lett.* **102**, 223001 (2009).
- [106] X. Wang and F. Robicheaux, Interference patterns from post-collision interaction in below-threshold photoexcitation auger processes, *Phys. Rev. A* **98**, 013421 (2018).
- [107] F. Maulbetsch and J. S. Briggs, Selection rules for transitions to two-electron continuum states, *J. Phys. B* **28**, 551 (1995).
- [108] W.-C. Jiang, S. Nagele, and J. Burgdörfer, Observing electron-correlation features in two-photon double ionization of helium, *Phys. Rev. A* **96**, 053422 (2017).